

Enhancement of spin polarization by chaos in graphene quantum dot systemsLei Ying¹ and Ying-Cheng Lai^{1,2}¹*School of Electrical, Computer, and Energy Engineering, Arizona State University, Tempe, Arizona 85287, USA*²*Department of Physics, Arizona State University, Tempe, Arizona 85287, USA*

(Received 9 November 2015; published 8 February 2016)

When graphene is placed on a substrate of heavy metal, the Rashba spin-orbit interaction of substantial strength can occur. In an open system such as a quantum dot, the interaction can induce spin polarization. Would classical dynamics have any effect on the spin polarization? Here we consider the quantum-dot setting, where the Rashba interaction is confined within the central scattering region whose geometrical shape can be chosen to yield distinct types of dynamics, e.g., regular or chaotic, in the classical limit. We find that as compared with regular or mixed dynamics, chaos can lead to significantly smooth fluctuation patterns of the spin polarization in its variation with the Fermi energy. Strikingly, in the experimentally feasible range of the Rashba interaction strength, the average polarization for a chaotic dot can be markedly larger than that for a regular or mixed dot. From the semiclassical viewpoint, a key quantity that determines the average spin polarization is the angle distribution of the outgoing electrons at the interface between regions with and without the Rashba interaction, respectively. Classical chaos generates a different distribution which, in turn, leads to higher average spin polarization. There was little previous work on the interplay between classical chaos and electron spin, and the phenomenon of chaos-enhanced spin polarization uncovered here can be exploited for spintronics applications.

DOI: [10.1103/PhysRevB.93.085408](https://doi.org/10.1103/PhysRevB.93.085408)**I. INTRODUCTION**

In a two-dimensional (2D) solid-state system, when the potential in the direction perpendicular to the 2D plane is asymmetric, the atomic spin-orbit coupling can lead to a momentum-dependent splitting of the spin bands, a phenomenon known as the Rashba effect [1] or the Rashba-Dresselhaus effect [2]. This effect can be exploited for manipulating spin in various settings such as electrical spin injection [3], 2D superconducting devices [4], spin modulation through an electrical field [5], spin filtering [6], and spin field effect transistor [7]. In two-dimensional Dirac materials of current interest such as graphene [8–13], topological insulators [14], and molybdenum disulfide (MoS₂) [15,16], intrinsic or extrinsic spin-orbit interactions of various degrees can arise. The interaction typically leads to energy splitting and can result in fascinating phenomena such as the spin Hall effect [17,18], weak antilocalization [19,20], spin-flipping scattering, and spin polarization [21–23]. There are two types of spin-orbit coupling: intrinsic and external. In graphene, the intrinsic spin-orbit coupling is usually quite weak, but significant interaction (e.g., characterized by energy splitting on the order of 200 meV) can be realized [24–26] through the Rashba effect by depositing graphene on the surface of Ni(111) or Ir(111). Rashba spin-orbit interaction preserves the time-reversal symmetry but breaks the inversion symmetry in the direction perpendicular to the two-dimensional material plane, and has wide applications in spin transport devices [27–33]. For example, for a two-terminal (source-drain) system with a Rashba field in the middle region, electrons of pure spin (say, spin up) are injected from the source and enter the central region. The Rashba coupling causes the electron spin to precess. When these electrons move into the drain terminal, some of them will have their spin flipped down. The flipping process leads to imperfect spin polarization. The degree of the spin polarization can then be modulated by the Rashba interaction strength.

In addition to the Rashba interaction strength, the geometric shape of the central interaction region can affect the electron scattering dynamics and, consequently, can have an effect on spin polarization. For convenience, we call the central region where the Rashba coupling exists the *scattering region*. Domains of different geometry can lead to characteristically distinct types of classical dynamics. For example, if the scattering region is rectangular, the underlying classical dynamics is integrable (or regular). However, a simple addition of two semicircular segments on two opposite sides of the rectangle leads to the stadium geometry, for which the classical dynamics is chaotic without any stable periodic orbits. If a small circular region at the center of a square is converted into a classically forbidden region (e.g., through the application of a localized electrical potential), then the domain becomes that of a Sinai billiard [34,35], for which the classical dynamics is fully chaotic with all periodic orbits being unstable. *The main result of this paper is that chaos can enhance spin polarization, a beneficial property that can be exploited for spintronics applications.*

We focus on a class of two-terminal graphene devices with Rashba interactions occurring in the central scattering region whose geometrical shape can be chosen to yield distinct types of dynamics in the classical limit. The shape of the scattering region is that of the cosine billiard [36–39] with upper and lower hard boundaries at $y(x) = W + (M/2)[1 - \cos(2\pi x/L - \pi)]$ and $y = 0$, respectively, for $-L/2 \leq x \leq L/2$. To make the scattering region symmetrical, we choose the lower boundary to be $y(x) = \pm W + (M/2)[1 - \cos(2\pi x/L - \pi)]$ for $-L/2 \leq x \leq L/2$, and the lead width is accordingly $2W$. The type of the classical dynamics in the billiard can be controlled by the parameter ratios W/L and M/L . For example, for $W/L = 0.18$ and $M/L = 0.11$, there are both stable and unstable periodic orbits, and the classical phase space is mixed (nonhyperbolic) with both chaotic regions and Kolmogorov-Arnold-Moser

(KAM) islands. However, for $W/L = 0.36$ and $M/L = 0.22$, all periodic orbits are unstable and the classical dynamics is fully chaotic (hyperbolic). Given a billiard shape, we construct the Hamiltonian incorporating Rashba interaction and use the Green's function method to calculate the conductance and spin polarization for systematically varied strength of the Rashba interaction. We find that classical chaos can not only smooth the fluctuations of the spin polarization with the Fermi energy, but, more importantly, can enhance the average spin polarization. We provide a heuristic argument based on semiclassical theory to understand the chaos-induced enhancement effect.

II. HAMILTONIAN AND CALCULATION OF SPIN POLARIZATION

In the tight-binding framework, the Hamiltonian of the graphene system with Rashba spin-orbit interaction (RSOI) is given [17] by $H = H_0 + H_R$, where the first and second terms describe the electron hopping and RSOI, respectively. The explicit forms of H_0 and H_R are

$$H_0 = -t \sum_{(i,j):\sigma} c_{i\sigma}^\dagger c_{j\sigma},$$

$$H_R = i \Delta_R \sum_{(i,j):\sigma,\bar{\sigma}} (s_{\sigma\bar{\sigma}} \times \mathbf{d}_{ij})_z c_{i\sigma}^\dagger c_{j\bar{\sigma}},$$
(1)

where, $c_{i,\sigma}^\dagger$ ($c_{j,\sigma}$) is the creation (annihilation) operator, σ ($\bar{\sigma}$) = \uparrow (\downarrow) or \downarrow (\uparrow), \mathbf{d}_{ij} is the vector from site i to site j , and $(\cdot)_z$ represents the z component of the vector quantity in parentheses. The hopping energy is $t = 2.8$ eV and Δ_R is the strength of the RSOI. We define the region with $\Delta_R > 0$ as the RSOI region. For convenience, we call the region for which $\Delta_R = 0$ the non-Rashba (NR) region.

The spin conductance of an open NR-RSOI-NR system can be calculated from the Green's function technique and the

classic Landauer-Büttiker formula,

$$G(E) = \frac{e^2}{h} \text{Tr}[\Gamma_L \mathcal{G}^r \Gamma_R \mathcal{G}^a],$$
(2)

where $\Gamma_{L(R)} = i[\Sigma_{L(R)}^r - \Sigma_{L(R)}^a]$, and $\mathcal{G}^{r(a)}$ is the retarded (advanced) Green's function of the central scattering region, which is given by

$$\mathcal{G}^r = (\mathcal{G}^a)^\dagger = [E - H_C - \Sigma_L^r - \Sigma_R^r]^{-1}.$$
(3)

We use the recursive Green's function method with high computational efficiency [40,41]. The conductance can be obtained as [30,42]

$$\mathbf{G}(E) = \begin{bmatrix} G_{11} & G_{12} \\ G_{21} & G_{22} \end{bmatrix},$$
(4)

where $G_{11(22)} = G_{\uparrow(\downarrow)} = G_{\uparrow\uparrow(\downarrow\downarrow)} + G_{\uparrow\downarrow(\downarrow\uparrow)}$ and the total conductance is given by $G_{\text{tot}} = G_{\uparrow} + G_{\downarrow}$. The nondiagonal element $G_{12(21)}$ contains the projection of the spin polarization into the (x, y) plane. The spin polarization $\mathbf{P} = [P_x, P_y, P_z]$ can be calculated through [31,42,43]

$$P_z = \frac{G_{11} - G_{22}}{G_{11} + G_{22}},$$

$$P_x - iP_y = \frac{2G_{21}}{G_{11} + G_{22}}.$$
(5)

III. NUMERICAL RESULTS

We vary two parameters: the Fermi energy E and the Rashba interaction strength Δ_R . The range of E is between zero and a fraction of t , the nearest-neighbor hopping energy of graphene, and the maximum value of Δ_R is set to be $0.07t \approx 200$ meV, which is the currently experimentally achievable value [24–26].

Effect of chaos and Rashba interaction on conductance and spin-polarization fluctuations. Figures 1(a) and 1(b) show the conductance fluctuation patterns with the Fermi energy for the

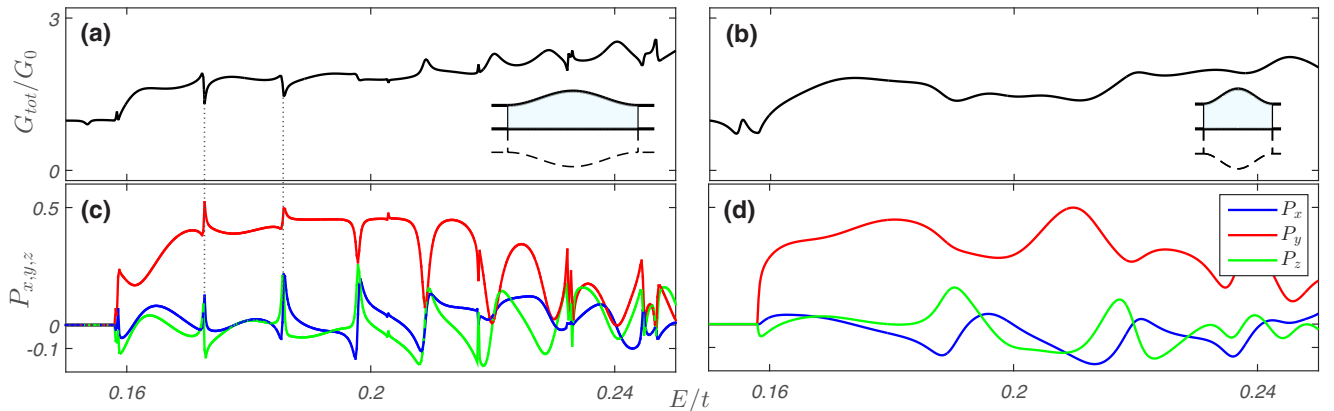


FIG. 1. The total conductance and spin polarization vs the Fermi energy for (a), (c) a nonhyperbolic and (b), (d) a hyperbolic graphene quantum dot. In both cases, the Rashba interaction strength is $\Delta_R = 0.07t \approx 200$ meV and the unit conductance is $G_0 = 2e^2/h$. The geometric parameters for the nonhyperbolic and hyperbolic dots are $(W/L = 0.18, M/L = 0.11)$ and $(W/L = 0.36, M/L = 0.22)$, respectively, with $W = 40a$ and $a = 0.142$ nm, and their dot shapes are illustrated in the insets in (a) and (b). The dashed boundaries are symmetrical with respect to solid boundaries about $y = 0$, and the scattering region is defined as the region in between the two vertical line segments. The blue, red, and green curves correspond to the x , y , and z components of the spin polarization. The gray dotted lines highlight the identical locations of the resonant peaks in the conductance and spin-polarization curves.

nonhyperbolic and hyperbolic dot systems, respectively, where the Rashba interaction strength is $\Delta_R = 0.07t \approx 200$ meV for both cases. For graphene quantum dots, a previous work [39] that did not treat Rashba interactions showed that fully developed chaos can eliminate sharp (Fano) resonances in the conductance curve and lead to smooth fluctuations. Comparing the conductance curves in Figs. 1(a) and 1(b), we see that the same holds: chaos can make the conductance fluctuations dramatically smoother even in the presence of Rashba interaction. A similar behavior occurs for all three components, $[P_x, P_y, P_z]$, of the spin polarization, as shown in Figs. 1(c) and 1(d). In particular, Fig. 1(c) exhibits Fano-like resonances in the spin polarization for the nonhyperbolic dot system, while the resonances entirely disappear when the classical dynamics becomes hyperbolic, as shown in Fig. 1(d). Note that in the window of the Fermi energy from $0.16t$ to $0.19t$, the y component of the spin polarization for the hyperbolic case maintains at a stable and relatively high level, $P_y \approx 0.4$, but this behavior does not occur for the nonhyperbolic system. As we will demonstrate, this stable region leads to a markedly higher value of the average spin polarization for the hyperbolic case as compared with the nonhyperbolic case. Note that the results shown in Fig. 1 are for zigzag boundaries in the horizontal direction. Since the average spin polarization is obtained over the energy range with two transverse modes (which is not close to the Dirac point), the edge type has little effect on the average spin polarization. In fact, our computations indicate that using armchair boundaries yields essentially the same result.

To understand the effect of chaos on fluctuations in the conductance and spin polarization, we calculate the width of the resonances [39,44] from the non-Hermitian Hamiltonian of the corresponding open system. In particular, the Hamiltonian H_C of the central scattering region is Hermitian with a set of real eigenvalues denoted as $\{E_{0\alpha}|\alpha = 1, \dots, N\}$, where N is the size of the Hamiltonian matrix (the number of carbon atoms in the graphene lattice in the scattering region). For the open system, the Hamiltonian matrix is $H_{\text{tot}}^c(E_0) = H_C + \Sigma_L^r(E_0) + \Sigma_R^r(E_0)$, where $\Sigma_L^r(E_0)$ and $\Sigma_R^r(E_0)$ are the complex self-energy matrices associated with the left and right leads, respectively, which characterize the coupling between the states in the scattering region and those in the leads. Solving the eigenvalues of $H_{\text{tot}}^c(E_0)$, we obtain a set of complex numbers $\{E_\alpha^c|\alpha = 1, \dots, N\}$, where $E_\alpha^c = E_{0\alpha} - \Delta_\alpha - i\gamma_\alpha$. The imaginary part of E_α^c characterizes the coupling strength between the states in the scattering region and in the leads, which effectively measures [39,45] the resonance width γ_α . If γ_α is small, e.g., less than $10^{-4}t$, a sharp, Fano-type resonance emerges in both the conductance and spin-polarization curves. If γ_α is relatively large, e.g., larger than $10^{-3}t$, the conductance and spin-polarization variations are smooth.

Figures 2(a)–2(d) show, for the nonhyperbolic and hyperbolic systems, the locations of various eigenvalues E_α^c in their own complex plane, for two cases where the Rashba interaction is absent and present with strength $0.07t$, respectively, where we choose $E_0 = 0.2t$ from the energy range in Fig. 1. Based on values of γ_α , qualitatively we can divide the complex plane into three regions: regions I–III, corresponding to $\gamma_\alpha < 10^{-4}t$, $10^{-4}t \leq \gamma_\alpha \leq 10^{-3}t$, and $\gamma_\alpha > 10^{-3}t$, respectively, which are specified with the dashed lines. Roughly, the values of γ_α

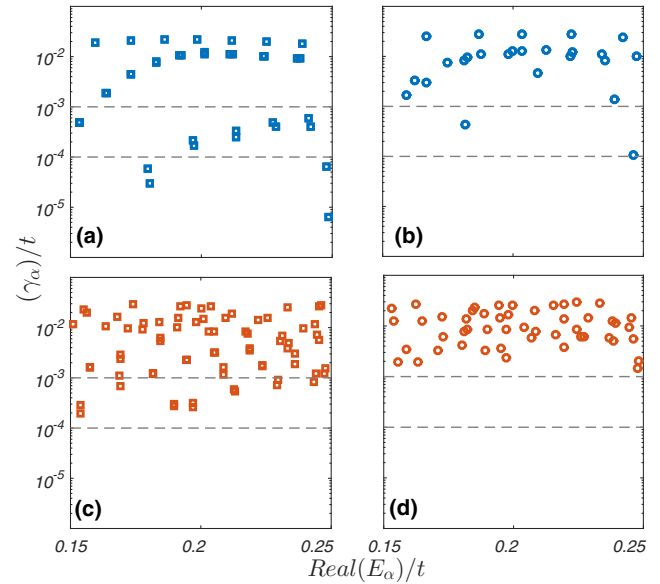


FIG. 2. Width of resonance γ_α for (a), (c) nonhyperbolic (squares) and (b), (d) hyperbolic (circles) quantum-dot systems. The Rashba interaction strength is (a), (b) $\Delta_R = 0$ and (c), (d) $\Delta_R = 0.07t$. Blue and red colors correspond to the cases where the Rashba interaction is absent and present, respectively. The gray dashed lines divide the complex plane of E_α^c into three regions for the purpose of qualitative analysis.

in regions I and II correspond to the Fano-like resonances in the conductance and spin-polarization curves [Fig. 1(c)], while those in region III correspond to the smooth variations [Fig. 1(d)]. For the nonhyperbolic dot, as shown in Figs. 1(a) and 1(c), without Rashba interaction, some values of γ_α are located in region I [Fig. 1(a)]. Generally, Rashba interaction can increase the width of the resonance [46]. In the presence of the interaction [Fig. 1(c)], the values of γ_α tend to increase slightly, but there are still a number of values in region II. For the hyperbolic dot, as shown in Figs. 1(b) and 1(d), without or with Rashba interaction, no eigenvalue is located in region I and almost no eigenvalues are in region II. In fact, almost all values of γ_α are located in region III, giving rise to smooth conductance and spin-polarization variations.

Signatures of the band splitting and the weak antilocalization effects can be seen in Fig. 2, which are caused by the RSOI. In particular, the Fano-type resonance is caused by the interplay between the quasidecrete energy levels from the quantum dot and the continuous background of the semi-infinite leads [47]. As the Rashba coupling strength is tuned up, a single discrete level splits into two. As a result, for both nonhyperbolic and hyperbolic quantum dots, the number of the Fano-type resonances doubles [cf., dot doubling in Figs. 2(c) and 2(d)]. However, we note that a sharp resonance corresponds to a pointer state in which the electrons are localized in the dot region, but the RSOI can smooth out the resonance. This is because of the weak antilocalization effect [19,20], which reduces the degree of localization and consequently broadens the width of the sharp resonances. In fact, as can be seen from Fig. 2, comparing with the case where there is no RSOI, the values of the imaginary eigenenergies γ_α with the RSOI in regions I and II are generally

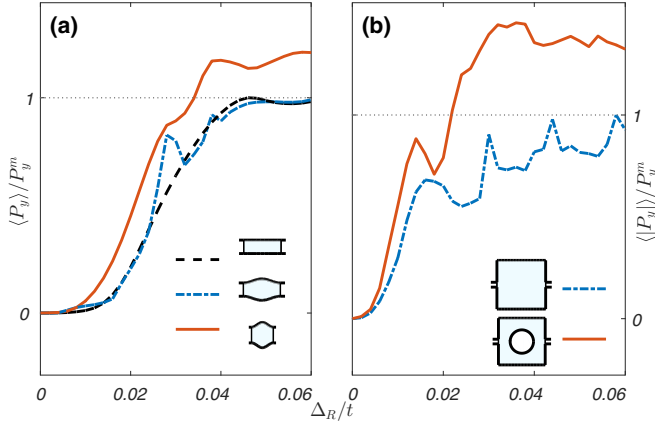


FIG. 3. Average spin polarization vs Rashba interaction strength (a) for integrable (black dashed curve), nonhyperbolic (blue dash-dotted curve), and hyperbolic (red solid curve) quantum dots, and (b) for rectangular (blue dash-dotted curve) and Sinai billiard (red solid curve) dot systems. The maximum spin polarization of integrable dots, P_y^m , is equal to (a) 0.347 and (b) 0.09. The side length of the rectangular billiard dot is $D = 118a$ and the lead width is $W = 6.5a$. The radius of the circular hard disk in the Sinai billiard system is $R = 0.258L$.

higher. In general, as the electron energy is increased, the total conductance will increase, reaching higher conductance plateaus [48].

Enhancement of spin polarization by chaos. In our coordinate setting, the y component of the spin polarization, P_y , is much larger than the x and z components. To be concrete, we focus on P_y . For both nonhyperbolic and hyperbolic dot systems, P_y fluctuates with the Fermi energy. A surprising finding is that for a relatively large energy interval, e.g., $0.15 \leq E/t \leq 0.25$, the average spin polarization tends to be larger for the hyperbolic system. For example, for $\Delta_R = 0.07t$, we have $\langle P_y \rangle \approx 0.275$ for the nonhyperbolic dot and $\langle P_y \rangle \approx 0.302$ for the hyperbolic dot. This is an indication that chaos can enhance the average spin polarization. The average spin polarization is obtained over the energy range covering two subbands. The reason to choose a relatively small lead width for the rectangular and the Sinai billiard systems in Fig. 3(b) was to reduce the effect of the lead on the scattering properties of the specific geometric domains to maximize the contrast between classical integrable and chaotic dynamics.

To obtain a better understanding of the role of chaos in enhancing spin polarization, we make the quantum-dot system symmetric in y so that the x and z components of the spin polarization vanish, while keeping the length of the scattering region unchanged [43]. Figure 3(a) shows $\langle P_y \rangle$ versus Δ_R for the symmetrical hyperbolic, nonhyperbolic, and integrable dot systems, where P_y is averaged over the energy range $0.083 \leq E/t \leq 0.141$ in which there are two modes in the leads. As Δ_R is tuned up from zero, $\langle P_y \rangle$ increases initially and then plateaus at a maximum value. For the integrable and nonhyperbolic dots, the curves of $\langle P_y \rangle$ versus Δ_R are nearly identical. The remarkable phenomenon is that the average spin polarization for the hyperbolic dot is consistently larger than that for the nonhyperbolic or integrable dots.

To demonstrate the generality of the phenomenon of enhancement of spin polarization by chaos, we study a characteristically different class of quantum-dot systems subject to Rashba spin-orbit interaction. In particular, a rectangular quantum dot, as shown in the inset of Fig. 3(b), has classically integrable dynamics. However, when a circular hard disk is introduced at the center of the rectangle, the classical dynamics becomes that of the Sinai billiard, which is fully chaotic [34,35]. The lead width is chosen to be small to minimize the effect of the leads on the scattering properties, so as to maximize the effect of the classical dynamics on spin transport. Calculations show that depending on the strength of the Rashba interaction, P_y can be either positive or negative. We thus focus on $\langle |P_y| \rangle$, where the average is again taken over the energy range in which the semi-infinite leads permit two modes: $0.696 \leq E/t \leq 0.965$. As shown in Fig. 3(b), the normalized $\langle |P_y| \rangle$ values (by its maximum for the integrable case) for the chaotic case are markedly larger than that for the integrable case, for all possible values of Δ_R . For $\Delta_R \approx 0.04t$, chaos-induced enhancement in the average spin polarization reaches maximum.

IV. SEMICLASSICAL ARGUMENT FOR ENHANCEMENT OF SPIN POLARIZATION BY CHAOS

In our system, a spin-up/-down electron enters the RSOI region from the left lead, where the Rashba interaction leads to spin precession. For simplicity, we assume that each scattering event changes only the propagation direction of the electron (as for the situation of classical reflection) and does not affect the spin precession. Due to the surface reflections experienced by the electron at the hard boundaries, the electron will scatter into the right lead with certain outgoing angle, on which the transmission coefficients t_{σ_R, σ_L} depend, where $\sigma_{L,R}$ denote the spin states at the left and right leads, respectively. The angle-dependent transmission coefficients give rise to angle-dependent spin polarization. Spin-polarization generation can then be treated as a refraction process at the RSIO-NR interface, as shown schematically in Fig. 4(a).

The Hamiltonian of a Dirac fermion with RSOI is given by $H = H_0 + H_R = \hbar v_F (\sigma_x k_x + \sigma_y k_y) + \Delta_R (\sigma_x s_y - s_x \sigma_y)$, where v_F is the Fermi velocity. The energy dispersion is given by $E = k$ for the NR region if we set $\hbar = v_F = 1$.

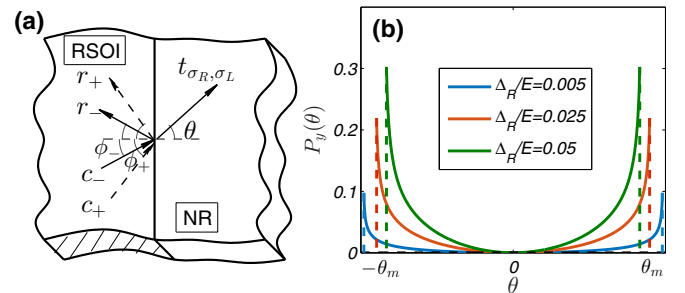


FIG. 4. (a) Schematic diagram of transmission behavior at the RSOI-NR interface. (b) The y component of the spin polarization, $P_y(\theta)$, vs the outgoing angle for $\Delta_R/E = 0.005$ (blue), 0.025 (red), and 0.05 (green). Dashed lines represent the maximum outgoing angles for different values of Δ_R/E .

In the RSOI region, due to the Rashba effect, the energy band splits into two subbands: $k_{\pm} = \sqrt{E^2 \mp E \Delta_R}$ and the eigenwave function is a linear superposition of the \pm states: $\Psi_R = c_+ \psi_+ + c_- \psi_-$, where c_{\pm} and ψ_{\pm} are the expansion coefficients and the eigenfunctions associated with the \pm states, respectively. Following a previous work [49], we set $c_+ = c_- = 1/\sqrt{2}$. The transmission coefficient t_{σ_R, σ_L} can then be obtained by imposing appropriate boundary conditions. The three components of the spin polarization are given by [30,43,50]

$$P_x - iP_y = \frac{2e^2/h}{G} \sum_{\sigma_L} t_{\uparrow\sigma_L} t_{\downarrow\sigma_L}^*, \quad (6)$$

$$P_z = \frac{(G_{\uparrow\uparrow} + G_{\uparrow\downarrow}) - (G_{\downarrow\uparrow} + G_{\downarrow\downarrow})}{G},$$

where the total conductance is given by $G_{\text{tot}} = G_{\uparrow\uparrow} + G_{\uparrow\downarrow} + G_{\downarrow\uparrow} + G_{\downarrow\downarrow}$ and $G_{\sigma_R \sigma_L} = e^2/h |t_{\sigma_R \sigma_L}|^2$. Figure 4(b) shows the y component of the spin polarization, P_y , versus the outgoing angle θ , where we observe a valley at the central region. As the RSOI strength is increased, the width of the valley in the P_y curve narrows down and the maximum value of P_y gradually increases. Note that $P_z(\theta)$ vanishes. For a system with an angular symmetry, we have $P_x(\theta) = P_x(-\theta)$ and, hence, $P_x(\theta)$ does not contribute to the spin polarization [43,50].

If the electronic wavelength is much smaller than the device size, i.e., $\lambda_e \ll L$, the electron motion can be described as that of a classical particle, rendering applicable a semiclassical approximation. For a chaotic domain, its boundary plays the role of random scattering sources for the electron. As a result, the electron trajectories extend all over the domain. Since the system is open, the electron has a finite average dwelling time τ_{dwell} in the RSOI region. However, for a nonhyperbolic/integrable domain, quantum pointer states [51–54] can arise. As a result, the classical quantity τ_{dwell} diverges. For the electrons that do escape, the angle distribution can be characteristically different from that of the chaotic case, as shown schematically in Figs. 5(a) and 5(b). To verify this, we numerically calculate the distribution of outgoing angles, $f(\theta)$, for both nonchaotic and chaotic systems, as shown in Fig. 5(c), where the classical particles are initialized from the left lead with their incident angles and y locations chosen randomly and uniformly. We see that f_{θ} is flatter for the chaotic domain and cosinelike for the nonchaotic domain. A fourth-order polynomial fit of the angle distribution gives $f_{\theta} = -0.057\theta^4 - 0.033\theta^2 + 0.416$ and $f_{\theta} = 0.024\theta^4 - 0.260\theta^2 + 0.504$ for the chaotic and nonchaotic domains, respectively.

The average spin polarization can be calculated from

$$\langle P_y \rangle = \frac{1}{2\theta_m} \int_{-\theta_m}^{\theta_m} f(\theta) P_y(\theta) d\theta, \quad (7)$$

where θ_m is the maximum outgoing angle, as indicated in Fig. 4(b). Figure 5(d) shows the average spin polarization versus Δ_R , where we see that for the chaotic device, it has higher values than those for the nonchaotic systems, in agreement with the numerical results in Fig. 3(a).

Figure 6(a) shows the outgoing angle distributions for the rectangular and Sinai billiard systems. For the former, the outgoing angle distribution is identical to that of the incident

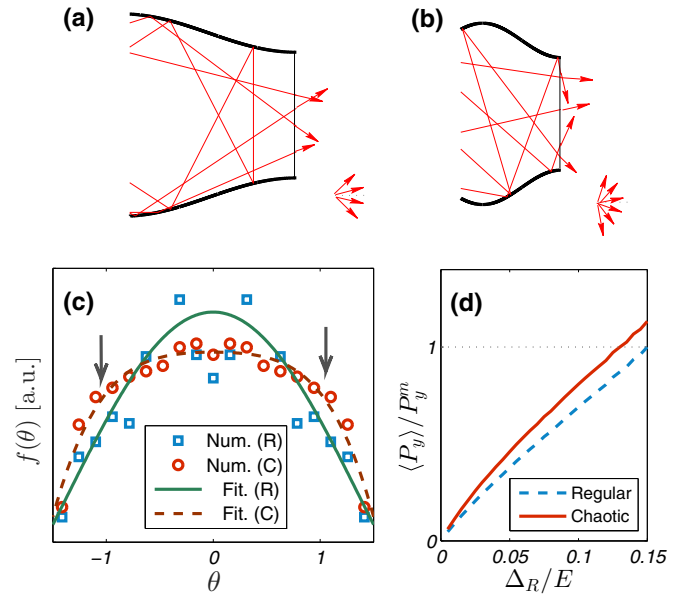


FIG. 5. (a), (b) Schematic illustration of classical outgoing trajectories for the nonchaotic and chaotic quantum-dot systems. (c) Numerically obtained angle distribution of the outgoing classical particles (blue: nonchaotic; red: chaotic), where the green solid and brown dashed curves are fourth-order polynomial fitting curves for the respective cases. (d) The average y spin polarization vs the RSOI strength (blue dashed curve: nonchaotic; red solid curve: chaotic). The maximum average spin polarization for the nonchaotic case is $P_y^m \approx 0.075$.

angles. For the Sinai system, the escaping probability is larger (smaller) for large (small) outgoing angles. The fitting functions are $f(\theta) = -0.120\theta^6 + 0.363\theta^4 - 0.284\theta^2 + 0.368$ and $f(\theta) = -0.775\theta^8 + 4.142\theta^6 - 7.059\theta^4 + 3.843\theta^2 + 0.056$ for the rectangular and the Sinai systems, respectively. Figure 6(b) shows the average spin polarization versus the RSOI strength for the two cases. In general, chaos has a more pronounced effect on spin polarization for large outgoing angles. When the angle distribution is taken into account, this leads to enhanced average spin polarization.

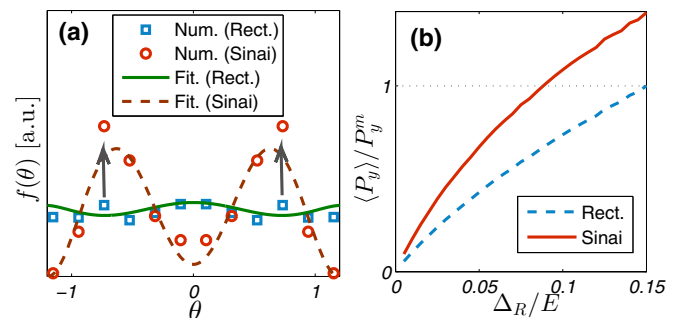


FIG. 6. (a) Angle distribution of the outgoing classical particles for the rectangular (blue squares) and Sinai (red circles) dot systems, with the respective polynomial fitting curves. (b) The y component of the average spin polarization vs the RSOI strength (blue dashed curve: rectangular dot; red solid curves: Sinai dot). The maximum average spin polarization for the rectangular system is $P_y^m = 0.0024$.

Would it be possible to obtain an explicit analytic expression for the average spin polarization? To address this question, we note that, in general, the spin polarization depends on the angle in a sophisticated way, and it seems not feasible to carry out the integration in Eq. (7) analytically so as to obtain an explicit formula for the average spin polarization. However, the behavior of the average spin polarization can be assessed by numerically integrating Eq. (7). Our results indicate unequivocally that the average spin polarization can be enhanced by chaos. Note that Eq. (7) is obtained based on semiclassical considerations, which is approximate with respect to the results from the tight-binding Hamiltonian. Practically, it may not be necessary to write down an explicit formula for the average spin polarization.

V. CONCLUSION AND DISCUSSION

Quantum chaos is referred to as the study of quantum manifestations of chaotic behaviors in the corresponding classical system [55,56], a field that has been extremely active for more than three decades. In the past decade, due to the tremendous development of the science of 2D Dirac materials initiated by the experimental realization of graphene [8–13,57], relativistic quantum manifestations of classical chaos [58] have emerged as a new field of study [39,59–64], with the basic goal to uncover and understand the possible role of chaos played in relativistic quantum systems. From a practical point of view, exploiting the interplay between chaos and relativistic quantum mechanics can lead to novel ideas for developing electronic devices.

This paper investigates the role of chaos in quantum transport in graphene systems subject to Rashba spin-orbit interaction (RSOI), an important quantum effect in solid-state systems [1,2]. Using the setting of a two-terminal graphene quantum dot where RSOI occurs in the central dot region, we focus on the average spin polarization, a key quantity in the study of spintronic devices. By varying the geometric shape of the dot region, we generate a spectrum of characteristically distinct classical behaviors such as integrable (regular), mixed, and fully developed chaotic dynamics. The quantum-dot setting thus represents a generic platform to study the interplay among classical chaos, RSOI, and relativistic quantum mechanics. We find that in the presence of RSOI, chaos can significantly reduce the sharp fluctuations in the spin polarization (e.g., as the Fermi energy is varied) that occur when the corresponding classical system is regular. A remarkable phenomenon is that in the experimentally feasible range of the variation of the Rashba interaction strength, the average spin polarization for the chaotic dot can be markedly larger than that for the regular or mixed dot. We develop a semiclassical understanding of the phenomenon of chaos-enhanced spin polarization. In particular, a key quantity that determines the average spin polarization is the angle distribution of the outgoing electrons at the interface between regions where RSOI is present and absent, respectively. We find that the angle distribution generated by classical chaos favors the spin alignments.

Our finding has practical value for developing graphene or other 2D Dirac material-based spintronic devices, such as nanoscale magnetic sensors using the mechanism of the Datta-Das transistor [65,66]. In particular, due to its high mobility and weak intrinsic spin-orbit coupling, graphene can preserve the spin orientation of spin-polarized electrons over long distances (e.g., $\sim 4 \mu\text{m}$ at room temperature and even up to $\sim 200 \mu\text{m}$ at low temperature) [67–72]. However, for a RSOI-based graphene device, the high spin-polarized currents can lead to variable magnetoresistances when the device is connected to a ferromagnetic material. The relatively large range of variation in the magnetoresistances can be used to develop magnetic sensors for reading magnetic information at a higher speed.

ACKNOWLEDGMENTS

We thank Dr. J.-F. Liu and Mr. G.-L. Wang for discussions. This work was supported by AFOSR under Grant No. FA9550-15-1-0151 and by ONR under Grant No. N00014-15-1-2405.

APPENDIX: CALCULATION OF SPIN POLARIZATION AT THE INTERFACES BETWEEN THE FREE AND RASHBA INTERACTION REGIONS

The continuous Hamiltonian of the Dirac fermion with RSOI is given by $H = \hbar v_F(\sigma_x k_x + \sigma_y k_y) + \Delta_R(\sigma_x s_y - s_x \sigma_y)$. There are two eigenvalues: $k_{\pm} = \sqrt{E^2 \mp E \Delta_R}$, with their normalized eigenwave functions given by

$$\psi_{\pm} = N_{\pm} \left[\begin{pmatrix} 1 \\ \frac{E}{k_{\pm}} e^{i\theta} \end{pmatrix} |\uparrow\rangle \pm i \begin{pmatrix} \frac{E}{k_{\pm}} e^{i\theta} \\ e^{2i\theta} \end{pmatrix} |\downarrow\rangle \right] e^{i\mathbf{k}\cdot\mathbf{r}}, \quad (\text{A1})$$

where $N_{\pm} = 1/\sqrt{2[1 + (E/k_{\pm})^2]}$ is a normalization constant and $\theta = \arctan(k_y/k_x)$. Due to the RSOI, the nondiagonal elements are finite and thus the ratio of the spin-up and -down state is equal to unity. The eigenwave function can be written as

$$\psi_{\uparrow,\downarrow} = \begin{bmatrix} 1 \\ e^{i\phi} \end{bmatrix} |\uparrow,\downarrow\rangle e^{i\mathbf{q}\cdot\mathbf{r}}. \quad (\text{A2})$$

The ratio can thus be arbitrary.

We consider a pure spin state incident from the left lead into the RSOI region and finally reaching the right-hand NR region, as shown in Fig. 4(a). The wave function in the RSOI and the right-hand NR regions can, respectively, be written as

$$\begin{aligned} \Psi_R &= c_+ \psi_+(\phi_+) + c_- \psi_-(\phi_-) + r_+ \psi_+(-\phi_+) \\ &\quad + r_- \psi_-(-\phi_-), \\ \Psi_N^{\sigma_L} &= t_{\sigma_L} \psi_{\uparrow}(\theta) + t_{\downarrow,\sigma_L} \psi_{\downarrow}(\theta). \end{aligned} \quad (\text{A3})$$

At the RSOI-NR interface ($x = 0$), the boundary condition is

$$\Psi_R(x) = \Psi_N^{\sigma_L}(x), \quad (\text{A4})$$

leading to solutions $[r_+, r_-, t_{\uparrow,\sigma_L}, t_{\downarrow,\sigma_L}]^T$, where we set $c_+ = c_- = 1/\sqrt{2}$ for the cases of $\sigma_L = \uparrow$ and \downarrow . As a result, we have $t_{\sigma_R,\uparrow} = t_{\sigma_R,\downarrow}$. Note that the coefficients satisfy the relation $r_+^2 + r_-^2 + t_{\uparrow,\sigma_L}^2 + t_{\downarrow,\sigma_L}^2 \approx c_+^2 + c_-^2$.

- [1] E. I. Rashba, *Sov. Phys. Solid State* **2**, 1109 (1960).
- [2] G. Dresselhaus and M. S. Dresselhaus, *Phys. Rev.* **140**, A401 (1965).
- [3] E. I. Rashba, *Phys. Rev. B* **62**, R16267 (2000).
- [4] L. P. Gor'kov and E. I. Rashba, *Phys. Rev. Lett.* **87**, 037004 (2001).
- [5] E. I. Rashba and A. L. Efros, *Phys. Rev. Lett.* **91**, 126405 (2003).
- [6] T. Koga, J. Nitta, H. Takayanagi, and S. Datta, *Phys. Rev. Lett.* **88**, 126601 (2002).
- [7] J. Schliemann, J. C. Egues, and D. Loss, *Phys. Rev. Lett.* **90**, 146801 (2003).
- [8] K. S. Novoselov, A. K. Geim, S. V. Morozov, D. Jiang, Y. Zhang, S. V. Dubonos, I. V. Grigorieva, and A. A. Firsov, *Science* **306**, 666 (2004).
- [9] K. S. Novoselov, A. K. Geim, S. V. Morozov, D. Jiang, M. I. Katsnelson, I. V. Grigorieva, S. V. Dubonos, and A. A. Firsov, *Nature (London)* **438**, 197 (2005).
- [10] Y. Zhang, Y.-W. Tan, H. L. Stormer, and P. Kim, *Nature (London)* **438**, 201 (2005).
- [11] A. H. Castro Neto, F. Guinea, N. M. R. Peres, K. S. Novoselov, and A. K. Geim, *Rev. Mod. Phys.* **81**, 109 (2009).
- [12] N. M. R. Peres, *Rev. Mod. Phys.* **82**, 2673 (2010).
- [13] S. Das Sarma, S. Adam, E. H. Hwang, and E. Rossi, *Rev. Mod. Phys.* **83**, 407 (2011).
- [14] M. Z. Hasan and C. L. Kane, *Rev. Mod. Phys.* **82**, 3045 (2010).
- [15] B. Radisavljevic, A. Radenovic, J. Brivio, V. Giacometti, and A. Kis, *Nat. Nanotechnol.* **6**, 147 (2011).
- [16] Q. H. Wang, K. Kalantar-Zadeh, A. Kis, J. N. Coleman, and M. S. Strano, *Nat. Nanotechnol.* **7**, 699 (2012).
- [17] C. L. Kane and E. J. Mele, *Phys. Rev. Lett.* **95**, 226801 (2005).
- [18] C. L. Kane and E. J. Mele, *Phys. Rev. Lett.* **95**, 146802 (2005).
- [19] S. Hikami, A. I. Larkin, and Y. Nagaoka, *Prog. Theor. Phys* **63**, 707 (1980).
- [20] T. Koga, J. Nitta, T. Akazaki, and H. Takayanagi, *Phys. Rev. Lett.* **89**, 046801 (2002).
- [21] R. Feder, *Phys. Rev. Lett.* **36**, 598 (1976).
- [22] M. Kalisvaart, M. R. O'Neill, T. W. Riddle, F. B. Dunning, and G. K. Walters, *Phys. Rev. B* **17**, 1570 (1978).
- [23] J. Kirschner and R. Feder, *Phys. Rev. Lett.* **42**, 1008 (1979).
- [24] Y. S. Dedkov, M. Fonin, U. Rüdiger, and C. Laubschat, *Phys. Rev. Lett.* **100**, 107602 (2008).
- [25] A. Varykhalov, D. Marchenko, M. R. Scholz, E. D. L. Rienks, T. K. Kim, G. Bihlmayer, J. Sánchez-Barriga, and O. Rader, *Phys. Rev. Lett.* **108**, 066804 (2012).
- [26] P. Leicht, J. Tesch, S. Bouvron, F. Blumenschein, P. Erler, L. Gragnaniello, and M. Fonin, *Phys. Rev. B* **90**, 241406 (2014).
- [27] F. Mireles and G. Kirczenow, *Phys. Rev. B* **64**, 024426 (2001).
- [28] L. W. Molenkamp, G. Schmidt, and G. E. W. Bauer, *Phys. Rev. B* **64**, 121202 (2001).
- [29] T. P. Pareek and P. Bruno, *Phys. Rev. B* **65**, 241305 (2002).
- [30] B. K. Nikolić and S. Souma, *Phys. Rev. B* **71**, 195328 (2005).
- [31] J.-F. Liu, Z.-C. Zhong, L. Chen, D. Li, C. Zhang, and Z. Ma, *Phys. Rev. B* **76**, 195304 (2007).
- [32] B. Srisongmuang, P. Pairor, and M. Berciu, *Phys. Rev. B* **78**, 155317 (2008).
- [33] Q. Zhang, Z. Lin, and K. Chan, *Appl. Phys. Lett.* **102**, 142407 (2013).
- [34] Y. G. Sinai, *Russ. Math. Surv.* **25**, 137 (1970).
- [35] Y. G. Sinai, *Introduction to Ergodic Theory* (Princeton University Press, Princeton, 1976).
- [36] G. A. Luna-Acosta, A. A. Krokhin, M. A. Rodríguez, and P. H. Hernández-Tejeda, *Phys. Rev. B* **54**, 11410 (1996).
- [37] B. Huckestein, R. Ketzmerick, and C. H. Lewenkopf, *Phys. Rev. Lett.* **87**, 119901(E) (2001).
- [38] H. Lee, C. Jung, and L. E. Reichl, *Phys. Rev. B* **73**, 195315 (2006).
- [39] R. Yang, L. Huang, Y.-C. Lai, and C. Grebogi, *Europhys. Lett.* **94**, 40004 (2011).
- [40] L. Ying, L. Huang, Y.-C. Lai, and C. Grebogi, *Phys. Rev. B* **85**, 245448 (2012).
- [41] L. Ying, L. Huang, Y.-C. Lai, and Y. Zhang, *J. Phys. Condens. Matter* **25**, 105802 (2013).
- [42] J.-F. Liu, K. S. Chan, and J. Wang, *Nanotechnol.* **23**, 095201 (2012).
- [43] F. Zhai and H. Q. Xu, *Phys. Rev. Lett.* **94**, 246601 (2005).
- [44] G.-L. Wang, L. Ying, Y.-C. Lai, and C. Grebogi, *Phys. Rev. E* **87**, 052908 (2013).
- [45] M. Mendoza, P. A. Schulz, R. O. Vallejos, and C. H. Lewenkopf, *Phys. Rev. B* **77**, 155307 (2008).
- [46] M. S. M. Barros, A. J. Nascimento Júnior, A. F. Macedo-Junior, J. G. G. S. Ramos, and A. L. R. Barbosa, *Phys. Rev. B* **88**, 245133 (2013).
- [47] A. E. Miroshnichenko, S. Flach, and Y. S. Kivshar, *Rev. Mod. Phys.* **82**, 2257 (2010).
- [48] W. Long, Q.-F. Sun, and J. Wang, *Phys. Rev. Lett.* **101**, 166806 (2008).
- [49] F. Liu, Y. Liu, J. Hu, D. L. Smith, and P. P. Ruden, *J. Appl. Phys.* **114**, 093708 (2013).
- [50] Q. Zhang, K. S. Chan, and Z. Lin, *J. Phys. D: Appl. Phys.* **47**, 435302 (2014).
- [51] R. Akis, D. K. Ferry, and J. P. Bird, *Phys. Rev. Lett.* **79**, 123 (1997).
- [52] L. Huang, Y.-C. Lai, D. K. Ferry, R. Akis, and S. M. Goodnick, *J. Phys. Condens. Matter* **21**, 344203 (2009).
- [53] D. K. Ferry, A. M. Burke, R. Akis, R. Brunner, T. E. Day, R. Meisels, F. Kuchar, J. P. Bird, and B. R. Bennett, *Semicond. Sci. Technol.* **26**, 043001 (2011).
- [54] R. Brunner, D. K. Ferry, R. Akis, R. Meisels, F. Kuchar, A. M. Burke, and J. P. Bird, *J. Phys. Condens. Matter* **24**, 343202 (2012).
- [55] H.-J. Stöckmann, *Quantum Chaos: An Introduction* (Cambridge University Press, New York, 1999).
- [56] F. Haake, *Quantum Signatures of Chaos*, 2nd ed. (Springer, Berlin, 2001).
- [57] C. Berger, Z. M. Song, T. B. Li, X. B. Li, A. Y. Ogbazghi, R. Feng, Z. T. Dai, A. N. Marchenkov, E. H. Conrad, P. N. First, and W. A. de Heer, *J. Phys. Chem. B* **108**, 19912 (2004).
- [58] M. V. Berry and R. J. Mondragon, *Proc. R. Soc. London Ser. A Math. Phys. Eng. Sci.* **412**, 53 (1987).
- [59] L. Huang, Y.-C. Lai, D. K. Ferry, S. M. Goodnick, and R. Akis, *Phys. Rev. Lett.* **103**, 054101 (2009).
- [60] L. Huang, Y.-C. Lai, and C. Grebogi, *Phys. Rev. E* **81**, 055203 (2010).
- [61] R. Yang, L. Huang, Y.-C. Lai, and L. M. Pecora, *Appl. Phys. Lett.* **100**, 093105 (2012).

- [62] H. Xu, L. Huang, Y.-C. Lai, and C. Grebogi, *Phys. Rev. Lett.* **110**, 064102 (2013).
- [63] L. Ying, G. Wang, L. Huang, and Y.-C. Lai, *Phys. Rev. B* **90**, 224301 (2014).
- [64] H.-Y. Xu, L. Huang, Y.-C. Lai, and C. Grebogi, *Sci. Rep.* **5**, 8963 (2015).
- [65] S. Datta and B. Das, *Appl. Phys. Lett.* **56**, 665 (1990).
- [66] E. W. Hill, A. K. Geim, K. Novoselov, F. Schedin, and P. Blake, *IEEE Trans. Magn.* **42**, 2694 (2006).
- [67] W. Han, K. Pi, K. M. McCreary, Y. Li, J. J. I. Wong, A. G. Swartz, and R. K. Kawakami, *Phys. Rev. Lett.* **105**, 167202 (2010).
- [68] P. Seneor, M.-B. Dlubak, B. and Martin, A. Anane, H. Jaffres, and A. Fert, *MRS Bull.* **37**, 1245 (2012).
- [69] W. Han, R. K. Kawakami, M. Gmitra, and J. Fabian, *Nat. Nanotechnol.* **9**, 794 (2014).
- [70] M. H. D. Guimarães, P. J. Zomer, J. Ingla-Aynés, J. C. Brant, N. Tombros, and B. J. van Wees, *Phys. Rev. Lett.* **113**, 086602 (2014).
- [71] M. Drögeler, F. Volmer, M. Wolter, B. Terrés, K. Watanabe, T. Taniguchi, G. Güntherodt, C. Stampfer, and B. Beschoten, *Nano Lett.* **14**, 6050 (2014).
- [72] M. V. Kamalakar, C. Groenveld, A. Dankert, and S. P. Dash, *Nat. Commun.* **6**, 6766 (2015).